Acoustic Purification of Extracellular Microvesicles

Kyungheon Lee,[†] Huilin Shao,[†] Ralph Weissleder,[†,‡] and Hakho Lee[*,†]

[†]Center for Systems Biology, Massachusetts General Hospital, 185 Cambridge Street, CPZN 5206, Boston, Massachusetts 02114, United States and
[‡]Department of Systems Biology, Harvard Medical School, Boston, Massachusetts 02115, United States

ABSTRACT Microvesicles (MVs) are an increasingly important source for biomarker discovery and clinical diagnostics. The small size of MVs and their presence in complex biological environment, however, pose technical challenges in sample preparation, particularly when sample volumes are small. We herein present an acoustic nanofilter system that size-specifically separates MVs in a continuous and contact-free manner. The separation uses ultrasound standing waves to exert differential acoustic force on MVs according to their size and density. By optimizing the design of the ultrasound transducers and underlying electronics, we were able to achieve a high separation yield and resolution. The "filter size-cutoff" can be controlled electronically *in situ*, which enables versatile MV-size selection. We applied the acoustic nanofilter to isolate nanoscale (<200 nm) vesicles from cell culture media as well as MVs in stored red blood cell products. With the capacity for rapid and contact-free MV isolation, the developed system could become a versatile preparatory tool for MV analyses.

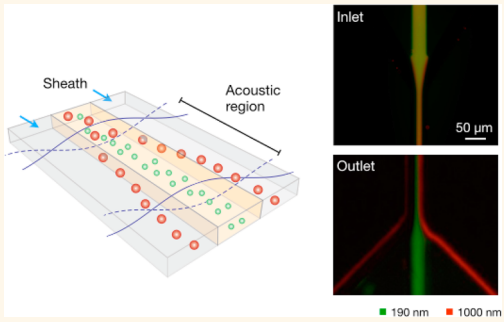

KEYWORDS: nanotechnology · microvesicles · nanoparticle separation · microfluidics · acoustic wave

With the growing recognition that microvesicles (MVs) can be harnessed for diagnostic purposes,[1,2] concomitantly increasing is the importance of separation technology to enrich these vesicles from biofluids. MVs are membrane-bound phospholipid vesicles (≤1 μm in diameter) and are actively secreted by mammalian cells into the circulation. The vesicles carry molecular constituents of their originating cells,[3−7] and are often viewed as partial surrogates of parental cells. Although MVs are abundant in the circulation (>10^{12} vesicles in 1 mL of blood), isolating intact MVs is still a challenging task because of their small size and presence in complex media. Conventional batch processes (*e.g.*, multiple filtration, ultracentrifugation) often require larger sample volumes, and entail time-consuming, extensive procedures,[8] which can lead to sample loss, and potential structural or molecular changes.

Acoustics-based microfluidics is a simple and yet robust strategy for on-chip particle manipulation.[9−15] The method generally uses ultrasound waves to exert radiation forces on particles; under the acoustic pressure, particles experience differential forces according to their mechanical properties (size, density, compressibility). The operation is label-free and can be performed without any physical contact between the field sources and fluidics. These advantages render the technology biocompatible and ideally suited for integration with microfluidics. Many different types of acousto-microfluidic systems have been developed to manipulate micrometer-scale (>1 μm) objects (*e.g.*, mammalian cells,[16,17] droplets,[18] microspheres[19] and platelets[20]). Acoustic separation of submicrometer MVs, however, has yet to be demonstrated. A major difficulty in such implementation is the requirement for high radiation force, arising from the small size and low compressibility of MVs.

We herein report on an acoustic nanofilter system developed to separate MVs from other contents of biological samples. We hypothesized that acoustic forces could be used to fractionate MVs according to their size, thereby enabling size-selective MV isolation on chip. The device was optimized, specifically in the design of ultrasound transducers and its electronics, to exert maximal acoustic force on MVs. We further

* Address correspondence to hlee@mgh.harvard.edu.

Received for review November 17, 2014 and accepted February 11, 2015.

Published online February 11, 2015
10.1021/nn506538f

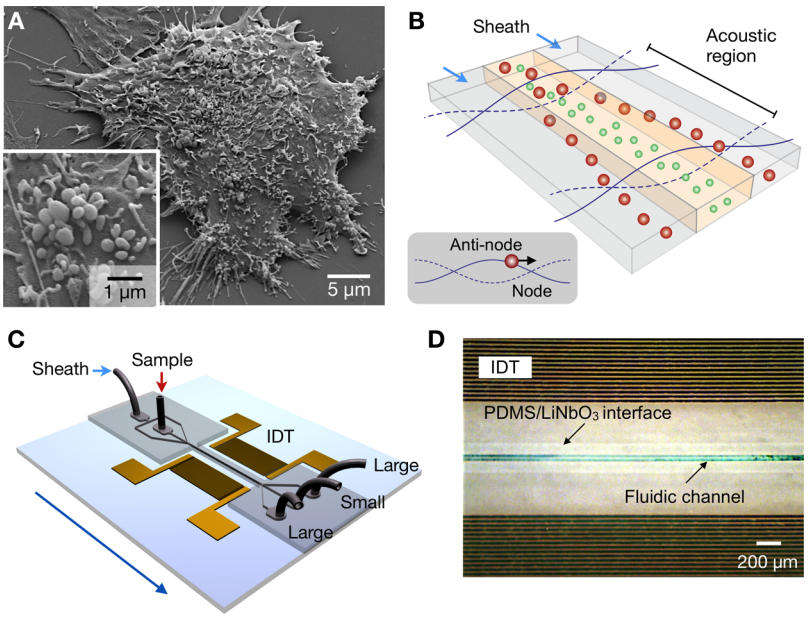

Figure 1. Acoustic nanofilter for label-separation of microvesicles (MVs). (A) Scanning electron microscopy image of MVs released by human brain tumor cells (GBM20/3). The size of MVs are typically <1 μm. (B) Filter operation. MVs in the acoustic region are under the acoustic radiation pressure and transported to nodes of acoustic pressure region (inset). Larger MVs move faster as the acoustic force is proportional to the MV volume. Sheath flows, positioned at the node region, remove large MVs, whereas the center flow retains small MVs. (C) Device schematic. A pair of interdigitated transducer (IDT) electrodes are used to generate a standing surface acoustic wave across the flow direction. Large MVs are collected at the two side outlets, and small MV at the center outlet. (D) Micrographs of a prototype device. The IDT electrodes were patterned on a piezoelectric ($LiNO_3$) substrate. The fluidic channel was permanently bonded to the substrate.

constructed an analytical model to fine-tune the size cutoff as well as to estimate the separation yields. The developed system was applied to sort different types of extracellular MVs. We isolated exosomes (diameter <200 nm) from cell culture medium and erythrocyte-derived vesicles from stored blood units. The operation was fast and simple: MVs were collected inside a single microfluidic device in a label-free, continuous and size-tunable manner. The developed system could be a versatile preparatory tool for MV analyses to further extend the utility of acoustofluidics.

RESULTS

Acoustic Nanofilter. The acoustic nanofilter was designed to separate extracellular MVs ($\leq$1 μm; Figure 1A) through in-flow size-fractionation. Figure 1B shows the operation principle. Particles in an acoustic field experience radiation forces and migrate toward the pressure nodes (Figure 1B, inset). The radiation force is proportional to the particle volume,[12] whereas the viscous drag to the particle size. Larger particle thus move faster to the pressure nodes, and can be transferred into sheath streams to exit. The cutoff size (d_c) can be determined *in situ* through the control of acoustic power and flow speed. Because the filtering is performed in a continuous-flow manner, the risk of channel clogging is minimized.

The device schematic is illustrated in Figure 1C. A pair of interdigitated transducer (IDT) electrodes are patterned, and used as an ultrasound source. The flow channel has two inlets for sample and sheath fluid, respectively, and is designed to focus the sample flow in the middle of the channel. The IDT electrodes generate a symmetric standing surface acoustic wave (SSAW) field across the channel direction, deflecting large particles toward the side outlets; small particles are collected at the center outlet.

We implemented a prototype device (Figure 1D) using $LiNbO_3$ piezoelectric wafer as a substrate. The IDT electrodes were patterned *via* standard lithography (see Materials and Methods for details). The fluidic structure, separately fabricated, was bonded to the SSAW chip (see Supporting Information (SI) Figure S1 for details on the device structure). We chose the acoustic wavelength λ = 100 μm to accommodate a wide channel width (60 μm) as well as to produce sufficient acoustic forces (>0.1 pN on 1-μm MVs). The resulting signal frequency for SSAW generation was 38.5 MHz. We further matched the impedance between IDT electrodes and the signal source to maximize the energy transfer. The frequency response of the IDT electrodes was measured, and the equivalent circuit was generated (SI Figure S2). We then used the *L*-matching network topology to transform the device impedance to that of a signal generator (50 Ω).

Analytical Model. We set up an analytical model for the implemented acoustic nanofilter. The acoustic force (F_a) on a spherical particle (diameter, d) can be expressed as[15]

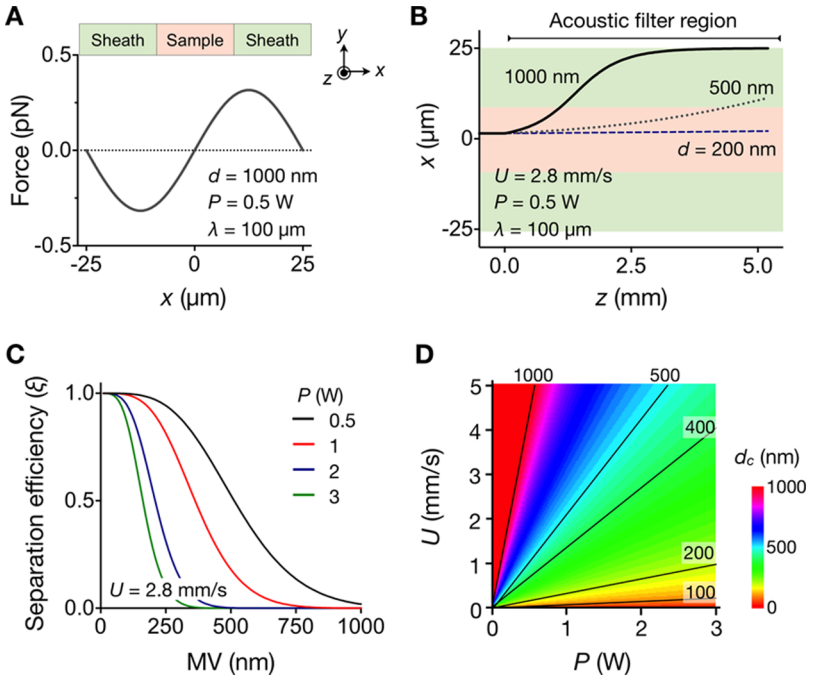

Figure 2. Analytical modeling of the implemented device. (A) Acoustic force (F_a) on MVs (diameter, d = 1000 nm) was calculated across the flow direction. Note that F_a has its maximum magnitude inside the sheath flow region. (B) Trajectories of MVs with different diameters were simulated along the flow stream (z-direction). The time for MVs to reach the sheath flow is $\sim d^{-2}$, which can be exploited for size-selective MV sorting. (C) The separation efficiency (ξ) was obtained by estimating the fraction of MVs collected in the center outlet. Higher RF input power (P) leads to enrichment smaller MVs. (D) The filter size cutoff (d_c) was obtained by imposing $\xi < 0.1$. The cutoff values can be set by controlling the input RF power (P) and the flow speed (U). For a given (P, U) setting, MVs with $d < d_c$ will be collected in the center channel. Representative d_c contour lines are shown. This map was used to set the device parameters in the subsequent experiments.

$$F_a = \frac{\pi^2 p^2 d^3}{12\lambda} \cdot \beta_m \cdot \phi \cdot \sin\left(\frac{4\pi}{\lambda} y\right)$$

where p is the acoustic pressure, β_m is the compressibility of the medium, and x is the particle position across the fluidic channel (Figure 2A). The acoustic pressure is further determined from the device characteristics, $p = (PZ/A)^{1/2}$, where Z is the acoustic impedance of the substrate, A is the IDT area, and P is the power of the input signal. The mechanical properties of MVs are represented by the acoustic contrast factor $\phi = (5\rho_p - 2\rho_m)/(2\rho_p + \rho_m) - (\beta_p/\beta_m)$, where ρ_p and β_p are the density and the compressibility of the particle, respectively, and ρ_m is the density of the media. Since $\phi > 0$, MVs in aqueous buffer move to the pressure nodes where F_a has its extremum values. The wavelength λ is thus controlled to position the nodes in the sheath flow region (Figure 2A).

The motion of MVs in a viscous flow can be obtained by solving $\mathbf{F_a} + \mathbf{F_d} = 0$ where $\mathbf{F_a}$ is the acoustic force and the $\mathbf{F_d}$ is the viscous drag (see Supporting Information for details). Figure 2B shows the simulated trajectory of MVs (ρ_p = 1130 kg/m^3, β_p = 3.5 × 10^{-10} Pa^{-1})[21] with different sizes (d = 200, 500, and 1000 nm) in an aqueous medium (ρ_m = 1000 kg/m^3, β_m = 5.1 × 10^{-10} Pa^{-1}). Because the acoustic force is proportional to the particle volume and the drag force to the particle diameter, larger MVs move faster to the pressure nodes. Indeed, the transit time (t_0) of MVs moving from the channel center to the sheath flow is $\sim 1/d^2$, which enables size-selective MV separation.

We further analyzed the separation efficiency (ξ). As an initial input, we assumed a monodisperse MV population (diameter, d) entering the sample channel. We then calculated the MV fraction collected at the center outlet after the acoustic filtration (SI Figure S3). Figure 2C shows ξ with varying MV size. For a given flow rate (U) and the channel length (L), higher input power (P) leads to steeper rejection of large MVs. By determining the minimum d value for $\xi < 0.1$, we then estimated the size cutoff (d_c) of the device (Figure 2D and Supporting Information). Note that the cutoff can be readily adjusted in the optimal size ranges (100−1000 nm) for MV fractionation, by controlling the operation parameters (P and U).

System Evaluation. We validated the device performance using polystyrene beads. Samples were prepared by mixing two differently sized, fluorescent polystyrene beads (green, d = 190 nm; red, d = 1000 nm) in phosphate buffered saline (PBS) solution. Prior to sample injection, the fluidic channel was surface-treated (0.1% F127 in PBS) to prevent nonspecific binding of particles. We set the operation parameters (P = 0.5 W, U = 2.8 mm/s) to achieve d_c = 470 nm; the acoustic contrast factor ϕ was 0.76, based on the density (ρ_p = 1050 kg/m^3) and the compressibility (β_p = 1.5 × 10^{-10} Pa^{-1}) of polystyrene beads.

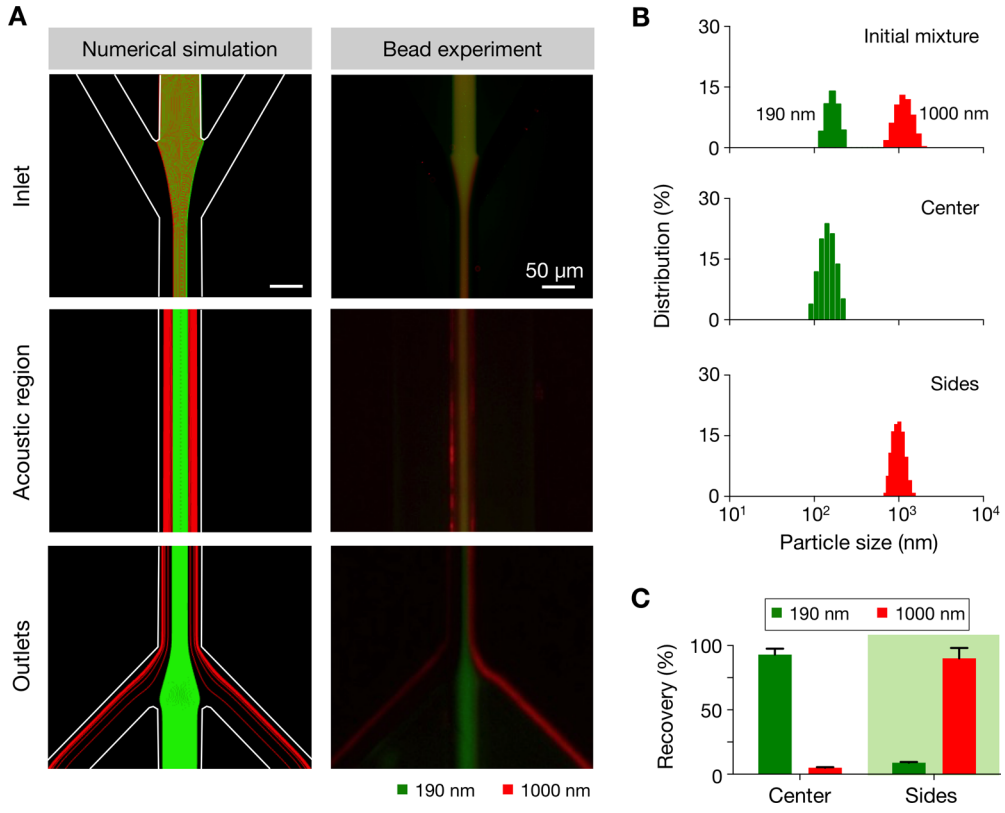

Figure 3. Filter validation with polystyrene particles. (A) Fluorescent particles of different size (d = 190 nm, green; d = 1000 nm, red) were mixed and processed by the acoustic nanofilter. Trajectories from the numerical simulation (left) and the experimental result (right) showed good agreement, with small and large particles respectively exiting to the center and the side outlets. (B) Particle size distribution measured by dynamic light scattering confirmed the size-selective enrichment of particles. (C) The recovery rate was estimated by comparing the fluorescence intensities of samples before and after the filtration. The observed recovery rate was >90% for both particles.

Fluorescence microscopy (Figure 3A, right) showed size-dependent separation of beads along the fluidic stream. Larger particles (red) migrated to the sheath streams and exited through the side outlets, whereas smaller particles (green) were collected at the center outlet (see SI Movie S1 for time-lapse images). The observed results agreed with those from hydrodynamic simulation (Figure 3A, left). The size distribution of particles, as measured by dynamic light scattering, further confirmed the device operation. We observed two distinct size groups in the initial mixture; these groups were correctly sorted in separate outlets after the acoustic nanofiltration (Figure 3B). The separation efficiency was determined from the fluorescence intensity of the collected particles and showed >90% for both small and large particles (Figure 3C). We further monitored the separation efficiency at different bead concentrations. Samples were prepared by spiking varying amounts of small beads (190 nm) into the suspension of large beads (1000 nm). The acoustic nanofilter maintained a consistent separation efficiency (>90%) with the dynamic range spanning 2 decades (SI Figure S4).

Exosome Purification. We next applied the acoustic nanofilter to enrich exosomes from other types of extracellular MVs. The size of exosomes is considered[1,22] < 200 nm. We thus tuned the device setting (P = 1.5 W, U = 1.5 mm/s) to set the size cutoff d_c = 300 nm for exosome isolation, using the acoustic contrast factor ϕ = 0.38 for lipid vesicles (ρ_p = 1130 kg/m^3, β_p = 3.5 × 10^{-10} Pa^{-1}).[21,22] For quantitative analyses, exosomes and larger MVs were prepared from cell culture media *via* filtration and ultracentrifugation (see Materials and Methods), and were independently labeled with green and red fluorescence, respectively. Known amounts of exosomes and larger MVs were then mixed and processed by the acoustic nanofilter.

Figure 4A shows the size distribution of samples measured by nanoparticle-tracking analysis (NTA) system. The initial mixture displayed two vesicle populations with their median diameter positioned at 149 and 410 nm, respectively. Following the acoustic filtration, the small and large particle populations were separated into the center and side outlets, respectively (see SI Figure S5 for electron micrographs). The recovery rates, estimated from fluorescence intensity measurements, were >80% for exosomes and >90% for larger MVs (Figure 4B). Western blotting (Figure 4C) and immunofluorescent microscopy (SI Figure S5b) further showed the enrichment of exosomes. Samples at the center outlet displayed high expression of exosomal markers, both extravesicular (CD63) and intravesicular (Flotillin-1, HSP70, HSP90), whereas the expression of

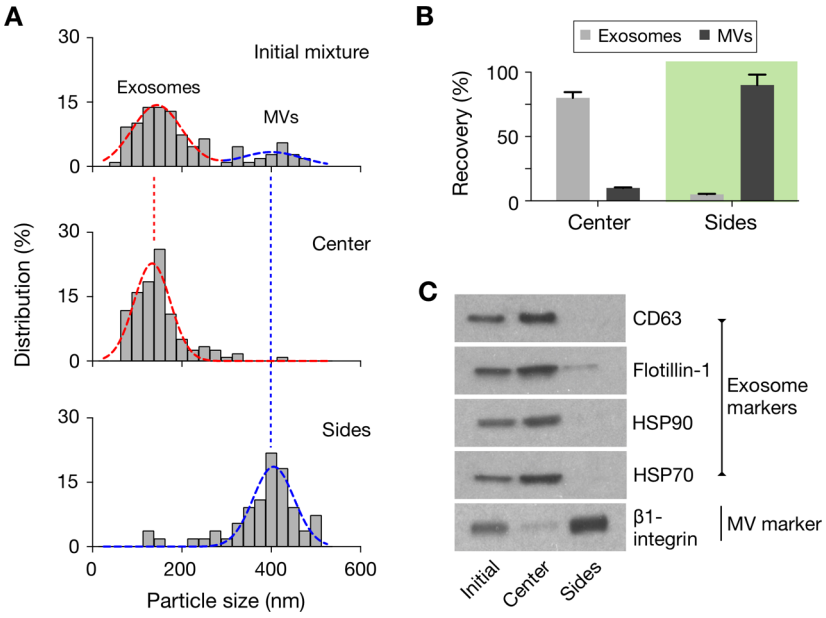

Figure 4. Exosome separation. (A) The acoustic nanofilter was used to separate exosomes (d < 200 nm) from other types of extracellular MVs. The size cutoff (d_c) was set to 300 nm by controlling P = 1.5 W and U = 1.5 mm/s (see Figure 2D). The size distribution of samples after the acoustic filtration was measured *via* nanoparticle tracking analysis (NTA), which showed the respective enrichment of small and large vesicles in the center and the side outlets. (B) The recovery rate was measured using a mixture of prestained exosomes and bigger MVs. (C) Western blotting further confirmed the enrichment of exosomes. Vesicles collected at the center outlet displayed high expression of exosome protein markers (CD63, Flotillin-1, HSP90, HSP70). MVs at the side outlets had high expression of β1-integrin, a marker for larger membrane MVs.

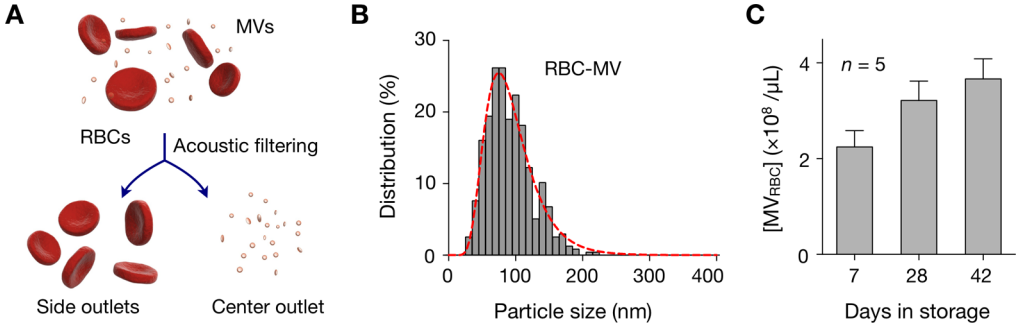

Figure 5. Monitoring of MVs in packed red blood cell (pRBC) units. (A) As a part of their aging process, red blood cells (RBCs) shed MVs. In stored pRBC units, MV numbers thus increase over time. The acoustic nanofilter was used to enrich RBC-derived MVs directly from pRBC samples. The size cutoff (d_c) was set to 450 nm. (B) The size distribution of collected MVs was analyzed by NTA. A single MV population with the mean d = 90.9 nm was observed. (c) The concentration of RBC-derived MVs [MV_{RBC}] was serially monitored in pRBC units (n = 5). The acoustic nanofilter was used to collect MVs from 10 μL of pRBC samples. The average [MV_{RBC}] value increased with the storage time.

other vesicular marker (Integrin β1) was low. The profile was reverse with MVs collected at the side outlets. The results also pointed to the vesicle integrity, demonstrating negligible acoustic damage from bubble cavitation.

MV Separation from Red Blood Cells. We further applied the acoustic filter to purify MVs in packed red blood cell (pRBC) units. As a part of their aging process, RBCs shed MVs (Figure 5A), effectively removing toxic, denatured hemoglobin and membrane proteins. In stored blood units, the number of these RBC-derived MVs increases over time.[23−25] MV separation and counting thus can be applied in monitoring the quality of blood products. To separate MVs from RBCs, we set the size cutoff d_c = 450 nm (P = 1.5 W, U = 2.5 mm/s). pRBC samples were directly processed by the acoustic filter. RBC-MVs were enriched at the center outlet, whereas RBCs were streamed to the side outlets. The size of the collected RBC-MVs was <200 nm (Figure 5B), in agreement with previous reports.[25] The performance of the acoustic filtration was as effective as that of a standard method (see Materials and Methods); the enriched MVs assumed a similar size distribution, and the separation yields were comparable (SI Figure S6). We also monitored the temporal changes of RBC-MV counts. Stored pRBCs units (n = 5) were sampled (10 μL per sample per time point) and processed at different time points. RBC-MVs were collected by the acoustic nanofilter.

RBC-MV numbers, measured by NTA, indeed significantly increased over time ($p < 0.03$, ANOVA), thereby confirming their potential as a metric of blood aging.

CONCLUSION

We have developed an acoustic-based microfluidic system for label-free and continuous filtration of MVs. We identified two key parameters which are important in assuring efficient manipulation: (i) high ultrasound frequency and (ii) efficient energy transfer to the sound transducer. We met these requirements by optimizing the transducer geometry (IDT electrodes) and by utilizing the impedance matching network. The resulting system achieved >90% separation yields, and allowed for *in situ* control of size cutoff. Analytical and numerical analyses validated experimental observations, and guided the setting of device parameters for specific MV targets.

The developed system could be a potential preparatory tool for MV analyses. Compared to conventional isolation methods (*e.g.*, ultracentrifugation, membrane filtration), acoustic filtering is fast, gentle on vesicles, and compatible with limited sample volumes. It also provides an easy approach to change the size-cutoff. In this study, we performed a binary separation (exosomes *vs* larger vesicles; microvesicles *vs* red blood cells). By cascading the separation regions with different size-cutoffs, it would be possible to differentiate multiple types of vesicles according to their size profile (*e.g.*, exosomes, oncosomes, apoptotic bodies).[21,26−28]

Several aspects of the system could be further developed to expand its functionality. First, different transducer designs, such as slanted-fingers[29] and tilted-angle electrodes,[30] could be investigated to better control the acoustic force and improve the sample throughput. Second, integrating analytical components (*e.g.*, sensors, polymerase chain reaction) into the same platform would be another promising approach to realize a portable lab-on-chip for MV analyses. Such advances will facilitate both clinical applications and biological studies of MVs, as well as extend the utility of acoustic microfluidics toward the nanoscale regime.

MATERIALS AND METHODS

Device Fabrication. The acoustic nanofilter consisted of two parts: a standing-surface-acoustic-wave (SSAW) chip and a microfluidic channel. The SSAW chip was fabricated on a piezoelectric substrate. A $LiNbO_3$ wafer with XY 128° cut was purchased (University Wafer). Interdigitated transducer (IDT) electrodes were patterned *via* conventional optical lithography, and metal layers (Ti, 50 Å; Au, 800 Å) were deposited. The patterned wafer was then cut into a desired size (21 mm × 21 mm) with a dicing saw. The microfluidic structure was fabricated in polydimethylsiloxane (PDMS; Dow Corning) *via* soft-lithography technique. The channel mold was formed on a Si wafer, using an epoxy-based photoresists (SU-8 2050, Microchem). The cross-section of the channel was 60 μm × 80 μm (width × height). Both the SSAW chip and the microfluidic block were treated with oxygen plasma, aligned and irreversibly bonded. We used ethanol as a temporary lubricant during the alignment. To strengthen the bonding, the assembly was cured on a hot plate (80 °C) for overnight.

System Setup. As a RF source, a signal generator (Agilent, N5158a) and power amplifiers (Mini circuits, TB-45) were used. The device operation was monitored by an inverted fluorescence microscope (Ti-E, Nikon). Images were recorded by a scientific-CMOS camera (Zyla 5.5, Andor) and analyzed by Image-J software.

Separation Assay with Polystyrene Particles. Fluorescent polystyrene particles with diameters of 190 nm (Dragon Green, Bangs laboratory) and 1000 nm (Flashred, Bangs laboratory) were used. Varying concentration of both particles were mixed in phosphate buffered saline (PBS) solution. Aliquots (50 μL) of the particle mixture were then processed by the acoustic nanofilter. The size distribution of particles at the sample inlet and outlets were measured by dynamic light scattering (Zetasizer Nano ZS, Malvern Instruments). To estimate the separation yields, the fluorescence intensities of the original and the separated samples were measured at the emission wavelength of 513 and 680 nm (Varian Cary Eclipse, Agilent).

Exosome Separation. Microvesicles (MVs) were isolated from cell culture. Human ovarian carcinoma cells (OvCA429, ATCC) were cultured in RPMI-1640 medium (Cellgro) supplemented with fetal bovine serum (FBS, Cellgro, 10%), penicillin and streptomycin (Cellgro, 1%), and L-glutamine (1%). Cells were cultured at 37 °C in a humidified atmosphere containing 5% CO_2. Cells at passages 1−15 were cultured in vesicle-depleted medium (with 5% depleted FBS) for 48 h. At their 70% confluence, conditioned culture medium was collected from ~10^7 cells and differentially centrifuged to isolated larger MVs as previously described.[7] In brief, the medium was filtered through a membrane filter (0.8 μm pore, Millipore) and centrifuged (10000*g*, 90 min). The pellet was retrieved as a large MV fraction.[31] Remaining supernatant was filtered through a 0.22-μm membrane filter (Millipore) and concentrated by differential centrifugation (100000*g*, 90 min) to isolate exosomes. Vesicle size was independently confirmed by the nanoparticle tracking analysis (NTA; LM10, NanoSight). Exosomes and larger MVs were labeled respectively with green and red fluorescent cell membrane dyes (PKH67 and PKH26, Sigma-Aldrich) before being mixed for sorting. The mixture (50 μL) was processed by the acoustic nanofilter. The sorted populations were analyzed for their size distribution and fluorescence intensity as described above.

Western Blotting. Isolated MVs were lysed in radio-immunoprecipitation assay buffer and supplemented with protease inhibitors (RIPA buffer, Thermo Scientific). MV samples were collected from the outlets of the microfluidic device and stored at −20 °C before analysis. Protein concentration was quantified using the bicinchoninic acid assay (BCA assay kit, Thermo Scientific). Protein lysates were loaded and resolved by sodium dodecyl sulfate polyacrylamide gel electrophoresis (SDS-PAGE) and transferred to PVDF membrane (Life Technologies). The PVDF membrane was then incubated overnight with antibodies against CD63 (Santa Cruz), Flotillin-1 (BD Biosciences), HSP90 (Cell Signaling), HSP70 (Cell Signaling) and β1-integrin (Cell Signaling). Following incubation with secondary antibody (Cell Signaling), enhanced chemiluminescence was used for detection.

MV Isolation from Stored Red Blood Cell (RBC) Units. Packed RBC (pRBC) units were obtained from the Massachusetts General Hospital (MGH) Blood Bank (Boston, MA). The units were preserved in Adsol solution, and stored at 4 °C. For serial MV monitoring, a 10-μL sample was drawn from each pRBC unit using a sterile coupler and 25G needle, after 7, 28, and 42 days of storage. All samples were used directly for sorting with the acoustic nanofilter. The standard MV samples were prepared *via* differential centrifugation steps (400*g* 20 min, 10000*g*, 3 min) followed by membrane filtration (0.22 μm pore). The size distribution and concentration of MVs were measured by NTA.

Conflict of Interest: The authors declare no competing financial interest.

Acknowledgment. The authors thank X. O. Breakefield (Massachusetts General Hospital) for access to and assistance with the NTA. The acoustic device was fabricated using the facilities at the Center for Nanoscale Systems (CNS) at Harvard University (National Science Foundation award ECS-0335765). This work was supported in parts by NIH Grants R01 HL113156 (H.L.), P01 CA069246 (R.W.), U54 CA151884 (R.W.), and DoD OCRP Award W81XWH-14-1-0279 (H.L.). This research was also partially supported by Basic Science Research Program through the National Research Foundation of Korea (NRF) funded by the Ministry of Education 2012R1A6A3A03040166 (K.L.)

Supporting Information Available: Design of the microfluidic system; impedance matching; MV distribution in the system; scanning electron micrographs of MV samples; separation efficiency measurement of exosome and MVs from pRBCs; supporting notes for analytical equations and movie. This material is available free of charge *via* the Internet at http://pubs.acs.org.

REFERENCES AND NOTES

1. Thery, C.; Ostrowski, M.; Segura, E. Membrane Vesicles as Conveyors of Immune Responses. *Nat. Rev. Immunol.* **2009**, *9*, 581–593.
2. Simpson, R. J.; Lim, J. W.; Moritz, R. L.; Mathivanan, S. Exosomes: Proteomic Insights and Diagnostic Potential. *Expert Rev. Proteomics* **2009**, *6*, 267–283.
3. Graner, M. W.; Alzate, O.; Dechkovskaia, A. M.; Keene, J. D.; Sampson, J. H.; Mitchell, D. A.; Bigner, D. D. Proteomic and Immunologic Analyses of Brain Tumor Exosomes. *FASEB J.* **2009**, *23*, 1541–1557.
4. Skog, J.; *et al.* Glioblastoma Microvesicles Transport RNA and Proteins That Promote Tumour Growth and Provide Diagnostic Biomarkers. *Nat. Cell Biol.* **2008**, *10*, 1470–1476.
5. Balaj, L.; Lessard, R.; Dai, L.; Cho, Y. J.; Pomeroy, S. L.; Breakefield, X. O.; Skog, J. Tumour Microvesicles Contain Retrotransposon Elements and Amplified Oncogene Sequences. *Nat. Commun.* **2011**, *2*, 180.
6. Valadi, H.; Ekstrom, K.; Bossios, A.; Sjostrand, M.; Lee, J. J.; Lotvall, J. O. Exosome-Mediated Transfer of Mrnas and Micrornas is a Novel Mechanism of Genetic Exchange Between Cells. *Nat. Cell Biol.* **2007**, *9*, 654–659.
7. Shao, H.; Chung, J.; Balaj, L.; Charest, A.; Bigner, D. D.; Carter, B. S.; Hochberg, F. H.; Breakefield, X. O.; Weissleder, R.; Lee, H. Protein Typing of Circulating Microvesicles Allows Real-Time Monitoring of Glioblastoma Therapy. *Nat. Med.* **2012**, *18*, 1835–1840.
8. Thery, C.; Amigorena, S.; Raposo, G.; Clayton, A. Isolation and Characterization of Exosomes from Cell Culture Supernatants and Biological Fluids. *Current Protocols in Cell Biology*; Wiley: New York, 2006; Chapter 3, No. Unit 3.22.
9. Bruus, H.; Dual, J.; Hawkes, J.; Hill, M.; Laurell, T.; Nilsson, J.; Radel, S.; Sadhal, S.; Wiklund, M. Forthcoming Lab on a Chip Tutorial Series on Acoustofluidics: Acoustofluidics-Exploiting Ultrasonic Standing Wave Forces and Acoustic Streaming in Microfluidic Systems for Cell and Particle Manipulation. *Lab Chip* **2011**, *11*, 3579–3580.
10. Yeo, L. Y.; Friend, J. R. Surface Acoustic Wave Microfluidics. *Annu. Rev. Fluid Mech.* **2014**, *46*, 379–406.
11. Shi, J.; Ahmed, D.; Mao, X.; Lin, S. C.; Lawit, A.; Huang, T. J. Acoustic Tweezers: Patterning Cells and Microparticles Using Standing Surface Acoustic Waves (SSAW). *Lab Chip* **2009**, *9*, 2890–2895.
12. Bruus, H. Acoustofluidics 7: The Acoustic Radiation Force on Small Particles. *Lab Chip* **2012**, *12*, 1014–1021.
13. Lenshof, A.; Magnusson, C.; Laurell, T. Acoustofluidics 8: Applications of Acoustophoresis in Continuous Flow Microsystems. *Lab Chip* **2012**, *12*, 1210–1223.
14. Lenshof, A.; Laurell, T. Continuous Separation of Cells and Particles in Microfluidic Systems. *Chem. Soc. Rev.* **2010**, *39*, 1203–1217.
15. Shi, J.; Huang, H.; Stratton, Z.; Huang, Y.; Huang, T. J. Continuous Particle Separation in a Microfluidic Channel *via* Standing Surface Acoustic Waves (Ssaw). *Lab Chip* **2009**, *9*, 3354–3359.
16. Ding, X.; *et al.* Standing Surface Acoustic Wave (Ssaw) Based Multichannel Cell Sorting. *Lab Chip* **2012**, *12*, 4228–4231.
17. Franke, T.; Braunmuller, S.; Schmid, L.; Wixforth, A.; Weitz, D. A. Surface Acoustic Wave Actuated Cell Sorting (SAWACS). *Lab Chip* **2010**, *10*, 789–794.
18. Franke, T.; Abate, A. R.; Weitz, D. A.; Wixforth, A. Surface Acoustic Wave (SAW) Directed Droplet Flow in Microfluidics for PDMS Devices. *Lab Chip* **2009**, *9*, 2625–2627.
19. Destgeer, G.; Lee, K. H.; Jung, J. H.; Alazzam, A.; Sung, H. J. Continuous Separation of Particles in a PDMS Microfluidic Channel *via* Travelling Surface Acoustic Waves (TSAW). *Lab Chip* **2013**, *13*, 4210–4216.
20. Nam, J.; Lim, H.; Kim, D.; Shin, S. Separation of Platelets From Whole Blood Using Standing Surface Acoustic Waves in a Microchannel. *Lab Chip* **2011**, *11*, 3361–3364.
21. Vader, P.; Breakefield, X. O.; Wood, M. J. Extracellular Vesicles: Emerging Targets for Cancer Therapy. *Trends Mol. Med.* **2014**, *20*, 385–393.
22. Thery, C.; Zitvogel, L.; Amigorena, S. Exosomes: Composition, Biogenesis and Function. *Nat. Rev. Immunol.* **2002**, *2*, 569–579.
23. Tissot, J. D.; Rubin, O.; Canellini, G. Analysis and Clinical Relevance of Microparticles from Red Blood Cells. *Curr. Opin. Hematol.* **2010**, *17*, 571–577.
24. Rubin, O.; Crettaz, D.; Canellini, G.; Tissot, J. D.; Lion, N. Microparticles in Stored Red Blood Cells: An Approach Using Flow Cytometry and Proteomic Tools. *Vox Sang* **2008**, *95*, 288–297.
25. Rho, J.; Chung, J.; Im, H.; Liong, M.; Shao, H.; Castro, C. M.; Weissleder, R.; Lee, H. Magnetic Nanosensor for Detection and Profiling of Erythrocyte-Derived Microvesicles. *ACS Nano* **2013**, *7*, 11227–11233.
26. EL Andaloussi, S.; Mager, I.; Breakefield, X. O.; Wood, M. J. Extracellular Vesicles: Biology and Emerging Therapeutic Opportunities. *Nat. Rev. Drug Discovery* **2013**, *12*, 347–357.
27. Di Vizio, D.; *et al.* Large Oncosomes in Human Prostate Cancer Tissues and in the Circulation of Mice with Metastatic Disease. *Am. J. Pathol.* **2012**, *181*, 1573–1584.
28. Morello, M.; *et al.* Large Oncosomes Mediate Intercellular Transfer of Functional Microrna. *Cell Cycle* **2013**, *12*, 3526–3536.
29. Bourquin, Y.; Syed, A.; Reboud, J.; Ranford-Cartwright, L. C.; Barrett, M. P.; Cooper, J. M. Rare-Cell Enrichment By a Rapid, Label-Free, Ultrasonic Isopycnic Technique for Medical Diagnostics. *Angew. Chem., Int. Ed. Engl.* **2014**, *53*, 5587–5590.
30. Ding, X.; *et al.* Cell Separation Using Tilted-Angle Standing Surface Acoustic Waves. *Proc. Natl. Acad. Sci. U. S. A.* **2014**, 12992–12997.
31. Witwer, K. W.; *et al.* Standardization of Sample Collection, Isolation and Analysis Methods in Extracellular Vesicle Research. *J. Extracell. Vesicles* **2013**, *2*, 20360.